Solar-Terrestrial Physics. 2025, vol. 11, iss. 4, pp. 64–71. DOI: 10.12737/stp-114202507.© 2025
I.V. Karpov, F.S. Bessarab, O.P. Borchevkina. Published by INFRA-M Academic Publishing House

DOI: 10.12737/stp-114202507

Received April 07, 2025
Accepted May 10, 2025

NUMERICAL MODELING OF SPATIAL PERTURBATIONS OF THE IONOSPHERE FROM LOCAL TROPOSPHERIC SOURCES

I.V. Karpov
West Department of Pushkov Institute of Terrestrial Magnetism, Ionosphere and Radio Wave Propagation RAS, Kaliningrad, Russia, ivkarpov@inbox.ru

O.P. Borchevkina
West Department of Pushkov Institute of Terrestrial Magnetism, Ionosphere and Radio Wave Propagation RAS, Kaliningrad, Russia, olga.borchevkina@mail.ru

F.S. Bessarab
West Department of Pushkov Institute of Terrestrial Magnetism, Ionosphere and Radio Wave Propagation RAS, Kaliningrad, Russia, bessarabf@gmail.com

Abstract. The paper presents the results of modeling of spatial and temporal perturbations of the thermosphere during a strong meteorological disturbance. The modeling was performed using the Global Self-Consistent Model of the thermosphere, ionosphere, and protonosphere (GSM TIP). The impact of tropospheric/stratospheric sources on the thermosphere during dissipation of acoustic and internal gravity waves, generated in the meteorological storm region, was considered in GSM TIP by specifying an additional thermal source. The results of modeling of ionospheric effects of the meteorological storm in October 2017 have shown that the action of a local additional source of heating of the thermosphere leads to perturbations of the thermosphere and ionosphere parameters both directly above the source region and at a significant distance from it. In additional heating of the thermosphere, a decrease is observed in the total electron content (*TEC*) values, reaching 20 % in the daytime compared to a meteorologically quiet day. To the south and east of the source region, there are positive *TEC* perturbations with relative amplitudes 5–10 % during the daytime. The physical processes determining the ionospheric response directly in the source region are conditioned by heating of the thermosphere and its influence on changes in the neutral composition and circulation of the neutral wind. The *TEC* perturbations in the regions remote from the source region are determined by dynamic processes, which lead to the eastward transport of plasma and displacement of ionospheric perturbations to low latitudes.

Keywords: total electron content, thermosphere, ionosphere, acoustic waves, internal gravity waves, numerical modeling, meteorological storm.

INTRODUCTION

Solar and geomagnetic activities are the main factors affecting ionospheric conditions; however, even with these factors being constant, the day-to-day variability of ionospheric parameters may run to 20 % [Lay, 2018; Pedatella, Liu, 2018]. Such variability is generally attributed to processes in the lower atmosphere, in particular, to severe meteorological disturbances in the troposphere, such as storms and typhoons [Chernigovskaya et al., 2015; Šindelárova et al., 2009; Hickey et al., 2001; Koucká Knížová et al., 2023; Bishop et al., 2006; Li et al., 2017; Wang et al., 2018]. Due to the high rate of occurrence of meteorological disturbances, their different spatial and time scales, as well as the complex pattern of their propagation from the troposphere to the upper atmosphere, it is often difficult to determine which disturbances in the lower atmosphere are associated with certain manifestations of the day-to-day ionospheric variability. The effect of meteorological disturbances on the ionosphere depends on their parameters, local time, season, and other factors. Physical mechanisms of these processes are as yet imperfectly understood, hence the need for further research into the ionospheric response to meteorological disturbances.

Of particular interest is to study the formation mechanisms of ionospheric irregularities, as well as the relationship of processes in the lower atmosphere with spatial and temporal manifestations of disturbances in the ionosphere. The main cause of such ionospheric disturbances is considered to be the generation and propagation of atmospheric waves of different scales: tidal, planetary, acoustic-gravity (see, e.g., [Wang et al., 2018; Koval et al., 2022]). The vertical interaction in the atmosphere that involves planetary waves has been studied in [Pancheva et al., 2013; Pedatella, Forbes, 2009]. Acoustic (AW) and internal gravity waves (IGW) play a special role in the vertical interaction between atmospheric layers. These waves propagate from the lower atmosphere to the upper atmosphere, where their dissipation leads to perturbations of the thermosphere and ionosphere [Hickey et al., 2001; Yiğit, Medvedev, 2015]. Experimental and theoretical studies confirm the important role of AW and IGW in transferring energy from the troposphere to the ionosphere [Artru et al., 2005; Hickey et al., 2011; Karpov et al., 2016; Koucká Knížová et al., 2020]. However, full understanding of these processes requires further research into the physical mechanisms of formation and dynamics of iono-

spheric irregularities resulting from tropospheric disturbances.

This paper presents the results of numerical modeling of spatiotemporal thermospheric and ionospheric perturbations caused by a local heat source in the thermosphere. This source simulates the heating that occurs during dissipation of AW and IGW generated in the region of a meteorological storm.

1. GSM TIP AND SETTING UP NUMERICAL EXPERIMENTS

Numerical experiments have been carried out using the Global Self-consistent Model of the thermosphere, ionosphere and protonosphere (GSM TIP). This physical model based on a finite-difference solution of a system of quasi-hydrodynamic equations for multicomponent plasma allows us to examine the key parameters of near-Earth space — electron density, temperature, and composition of ions and neutral gases, as well as their changes caused by solar activity, geomagnetic storms, and artificial influences.

GSM TIP takes into account the interaction of charged particles (ions and electrons) with neutral gases, as well as the effect of electric fields of magnetospheric and dynamo origin. The model calculates the following near-Earth space parameters: electron density, concentrations of ions (O^+, H^+, NO^+, O_2^+, N_2^+), electron and ion temperatures, ion velocity vector components; electric fields of magnetospheric and dynamo origin; concentrations of the main components of neutral composition (O_2, N_2, O) and odd nitrogen (NO, $N(^2D)$, $N(^4S)$); neutral gas temperature; components of the mean mass velocity vector. GSM TIP is detailed in [Namgaladze et al., 1991; Korenkov et al., 1996; Bessarab, Koren'kov, 1998; Klimenko et al., 2006].

The model is employed to study diurnal, seasonal, and solar-cyclic variations in the upper atmosphere parameters, as well as the effects of geomagnetic disturbances on the ionosphere and thermosphere [Klimenko et al., 2011; Klimenko et al., 2016; Yasyukevich et al., 2018].

The numerical experiments discussed in this paper were carried out for geomagnetically quiet conditions on October 28–30, 2017, when there was a powerful meteorological storm over the European continent. Figure 1 presents maps of surface pressure in the region of the meteorological storm passage according to the ERA5 reanalysis data [Hersbach et al., 2020]. The eye of the cyclone (minimum pressure) is seen to form over the Mediterranean Sea. The meteorological storm slowly moves to the northeast, reaches its maximum over Central Europe on October 29–30, and decays over Northern Europe by noon on October 31. The maximum wind gusts in the Kaliningrad Region were as strong as 27 m/s in the second half of October 29 – the first half of October 30, which allows us to classify this meteorological disturbance as strong — Beaufort Force 8–9.

In GSM TIP, the lower boundary is at an altitude of 80 km, so it is impossible to examine *in situ* ionospheric effects from phenomena occurring in the underlying atmosphere. The disturbances coming from the troposphere and stratosphere cannot be correctly accounted for by setting appropriate boundary conditions at the altitude of 80 km due to the absence of fast wave processes in the large-scale hydrostatic model GSM TIP. Assuming that in the real thermosphere short IGWs propagating from below dissipate in the altitude range ~120–150 km, the effect of tropospheric/stratospheric sources in the thermosphere in GSM TIP can be taken into account by specifying a heat source at the height of the estimated

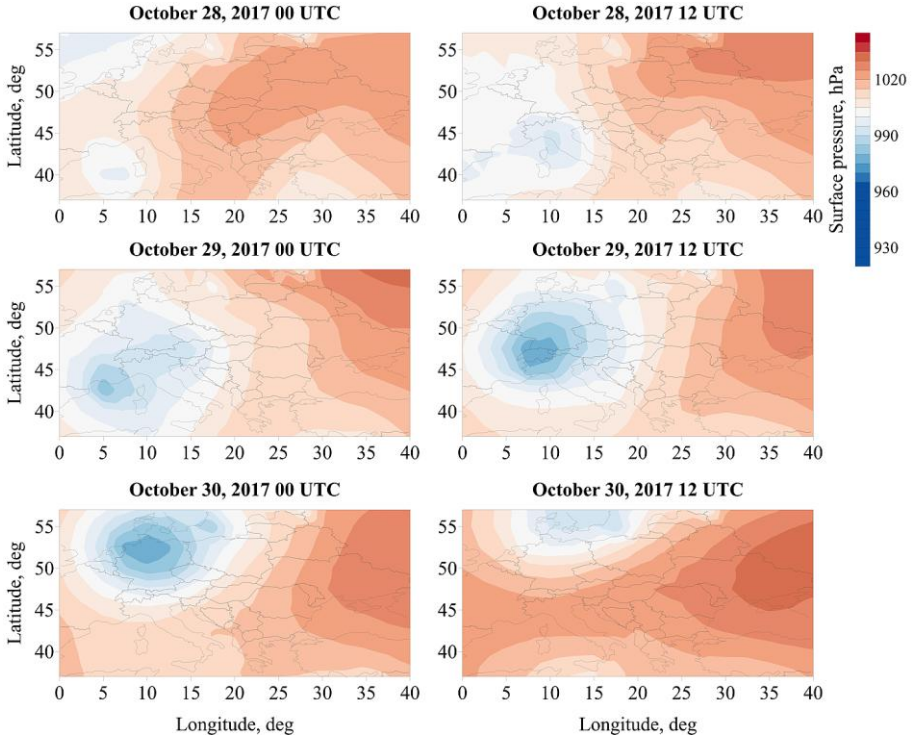

Figure 1. Surface pressure in the region of storm passage at different time points on October 28–30, 2017

maximum dissipation [Karpov et al., 2020]. For this purpose, in the calculation with a heat source, a temperature disturbance (ΔT) is added to the calculated temperature at each time step. In some cases, a meteorological disturbance may have a complex spatial pattern that can be modeled by superposition of sources described by the expression of the form $\sum_{i=1}^{N} A_i Q_i(\theta, \varphi, t) S_i(h)$. Here N is the number of specified sources; A_i is the amplitude of the ith thermal disturbance, selected so that the integral action of the source during its existence (inclusion) reaches the required thermal effect; $Q_i(\theta, \varphi, t)$ is the latitude-longitude distribution of the ith source; $S_i(h)$ is its altitude distribution, which is calculated from $\exp\left(-(h-h_{0i})^2/\Delta h_i^2\right)$; h_{0i} and Δh_i were 120 km and 20 km respectively. In this paper, the thermal effect of the October 28–30 meteorological disturbance was modeled by three sources with the same amplitude and height dependence. The position of the sources in grid nodes of the model and the number of simultaneously active sources were set so that their superposition approximately repeated the geographic location and motion of the meteorological storm (see Figure 1). The activation time of the sources is 18 UT on October 28, and the time of their deactivation is midnight on October 30. The sources' normalized amplitude of 1.2 K/min was selected so that the maximum temperature ranged up to ~100 K at an altitude of 300 km.

2. CALCULATION RESULTS

The input parameters of GSM TIP are geomagnetic and solar activity indices. In the presented numerical experiments, these indices did not change, hence the perturbations obtained in the calculations were caused only by additional thermal sources simulating the result of IGW dissipation in the thermosphere. GSM TIP made the calculations for the conditions of October 28–30, 2017 with an additional heat source (variant 1 — B1) and without it (variant 2 — B2). To identify the effects caused by the additional heat source in the thermosphere, we examined perturbations of the thermosphere and ionosphere parameters, which were calculated as the difference between their values in variants 1 and 2:

$$del(n_p, r, \theta, \varphi, t) = \\ = Rez1(n_p, r, \theta, \varphi, t) - Rez2(n_p, r, \theta, \varphi, t),$$

where n_p is the parameter number; r is the altitude; θ and φ are latitude and longitude; t is the time; $Rez1(n_p, r, \theta, \varphi, t)$ and $Rez2(n_p, r, \theta, \varphi, t)$ are arrays of calculation results for variants 1 and 2.

Figure 2 shows a pattern of changes in relative temperature perturbation $(T_n(B1)–T_n(B2))/T_n(B2)$ with time for a point with coordinates 40° N, 10° E. The heating activation time and the formation of a local temperature increase at an altitude of 120 km, where the maximum of the source is located, as well as regions of lower T_n at 135–140 km are clearly visible. Time variations in the source power generate dynamic processes that begin to affect the entire thermosphere above the source, heating the neutral gas above 140 km. Since the heat capacity of neutral gas decreases significantly with height, a relatively small heating at 120 km leads to a significant increase in temperature in the upper thermosphere, which persists after the end of the meteorological storm in the troposphere.

Propagation of the temperature perturbation during the meteorological disturbance at an altitude of 200 km in the Northern Hemisphere is demonstrated in Figure 3. The activation time of the source, a change in its amplitude and spatial configuration generate wave-like heat propagation from the epicenter of the meteorological storm to high and low latitudes. The temperature effect, insignificant on October 28 — about ± 10 K, increases a day later, on October 29. The area of maximum heating covers most of the Northern Hemisphere and moves first from the epicenter to high latitudes, and then to low latitudes. The heating area increases on October 30, the process of heat transfer to high latitudes and back is repeated, and ΔT_n exceeds 50 K. In the calculations, the heat source is nonstationary and the temperature perturbation it generates at the altitude of 200 km is alternating; the positive effect begins to dominate after noon on October 29 (see Figure 3).

A significant increase in temperature in the F2-region perturbs ionospheric parameters. Study of total electronic content (*TEC*) variations during different heliogeophysical events is a widely used and available

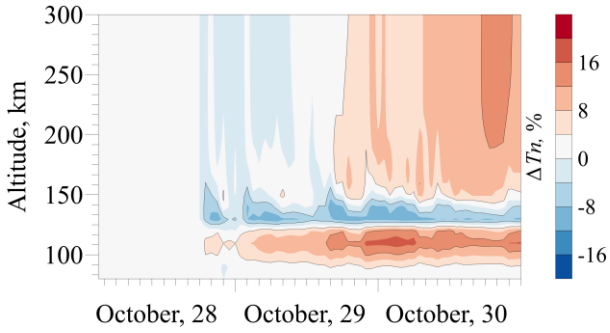

Figure 2. Change of relative temperature perturbation $(T_n(B1)–T_n(B2))/T_n(B2)$ in the time–altitude plane for a point with coordinates 40° N, 10° E

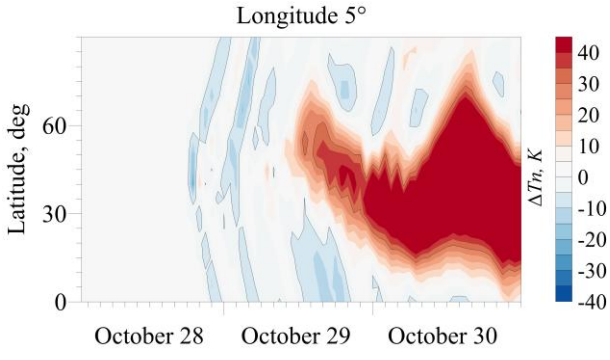

Figure 3. Change of temperature perturbation ΔT_n at an altitude of 200 km at 5° E in the Northern Hemisphere on October 28–30, 2017

tool for monitoring the ionosphere [Zakharov, Kunitsyn, 2012; Astafyeva, 2019; Rahmani et al., 2020]. The nonlocal pattern of the ionospheric disturbance is well illustrated by time variations in the perturbation of the model total electron content (Δ*TEC*) at longitudes of 5° and 50° E (Figure 4). Recall that the perturbation of the parameters was calculated as the difference between the values in two calculation variants — with and without regard to the additional source. The disturbance amplitude is seen to increase during the daytime and decrease at night, with negative disturbances prevailing, which are as strong as –5 TECU at 5° E on October 30. At 50° E, there are smaller variations Δ*TEC*, which also intensify on October 30, reaching –3 TECU. In addition to the negative disturbance, there are small positive perturbations in Δ*TEC* variations at equatorial latitudes.

Figure 5 displays Δ*TEC* in the Northern Hemisphere, plotted for October 29 and 30 at 12:00 UTC. The *TEC* perturbations are seen to manifest themselves both in the region of the additional heat source and at a considerable distance from it. Negative *TEC* perturbations propagate mainly in a southerly direction, and a region of a slight increase in *TEC* is formed southeast of the epicenter. The disturbance amplitude is ~2 and 5 TECU during the daytime on October 29 and 30 respectively. The night Δ*TEC* values are negligible and are not given here.

The calculated maps of Δ*TEC* variations can be compared with *TEC* perturbations obtained from global maps of total electron content based on data from navigation satellite systems. Figure 6 illustrates Δ*TEC* perturbations plotted using CODE (Center of Orbit Determination in Europe) maps [Schaer, 1999]. Background unperturbed *TEC* was formed as average 8 days before the meteorological storm, from October 20 to October 27. Δ*TEC* was the largest on October 30 (Figure 6). Above 30° N, there is a pronounced region of negative Δ*TEC*~–4 TECU, which formed approximately above the eye of the cyclone considered. As in the model calculations (see Figure 5), the TEC perturbation is shifted in longitude by 10°–20° to the west of the source. Note that the significant decrease in Δ*TEC* at low latitudes and at the equator is probably caused by the difficulty in reconstructing the equatorial anomaly on TEC maps.

3. DISCUSSION

Ionospheric disturbances are obviously generated by an additional heat source in the thermosphere, which simulates the effect of propagation and dissipation of waves coming from the lower atmosphere. The appearance of regions of higher temperature affects ionization-recombination processes and causes the electron density to decrease. The physical processes developing under the influence of local thermal sources in the thermosphere and their effect on the ionosphere are carefully examined in [Hickey et al., 2001; Karpov and Vasiliev, 2020; Gavrilov et al., 2020; Kurdyaeva et al., 2024]. Local heating of neutral gas leads to corresponding increases in pressure and anticyclonic dynamics. Figure 7 depicts the distribution of disturbances of thermospheric wind horizontal components in the Northern Hemisphere at an altitude of 250 km for different time points on October 29 and 30.

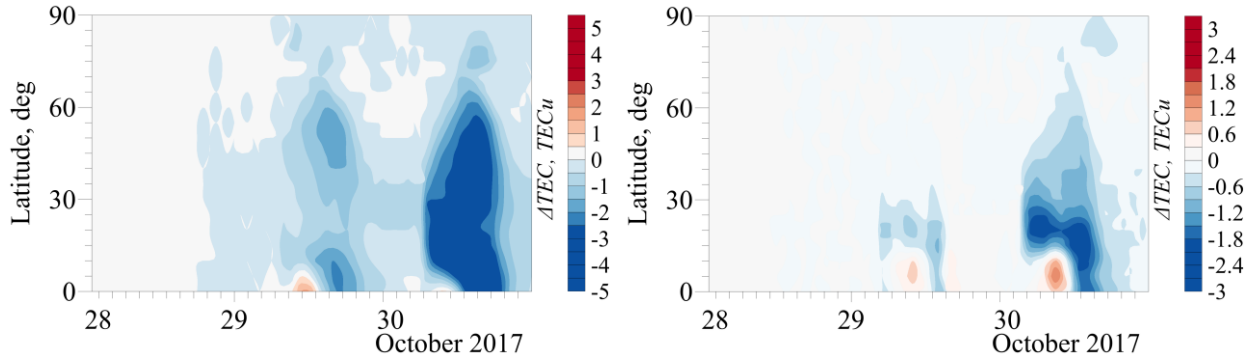

Figure 4. Variations in model Δ*TEC* at 5° E (*a*) and 50° E (*b*) in the Northern Hemisphere

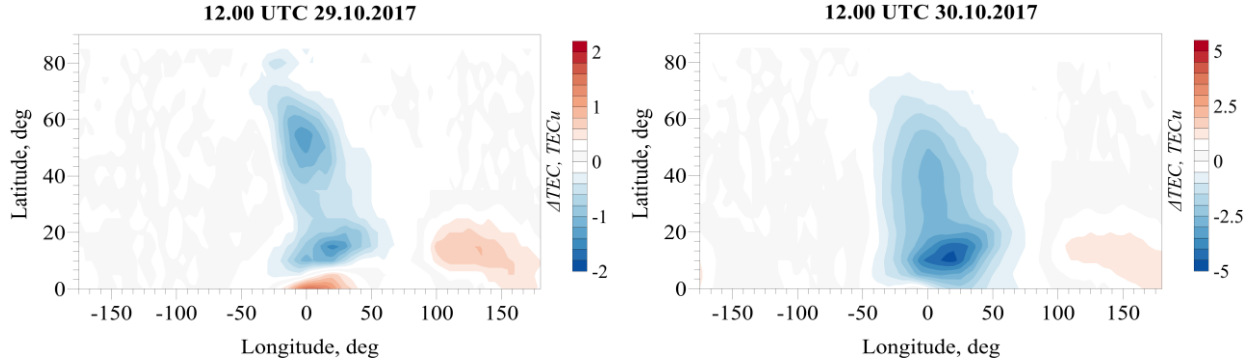

Figure 5. Distributions of Δ*TEC* perturbations in the Northern Hemisphere at 12:00 UT on October 29 (*a*) and 30 (*b*), 2017

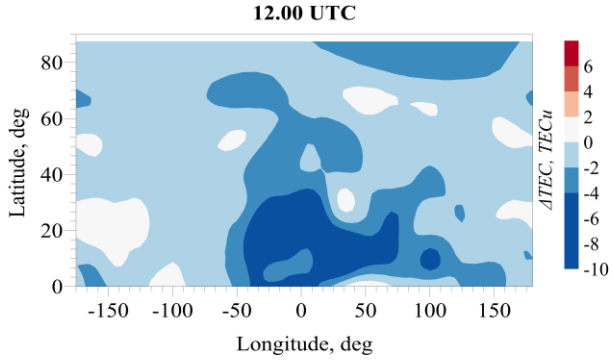

Figure 6. Total electron content perturbations in the Northern Hemisphere on October 30, 2017 at 12:00 UT, plotted from CODE maps

The wind disturbances are seen to be irregular directly above the heat source during the first hours of its operation. During further operation of the source in daytime conditions, vortex structures appear. Thus, an anticyclonic disturbance occurs to the west of the source (0°–100° W); and at longitudes 0°–50° E north of the source, the disturbance is cyclonic. At night from –50° W to 50° E, the wind disturbance is directed toward the equator. Note also that during operation of the source a zonal flux directed to the east is formed over time. In general, the wind disturbance is determined by two main processes caused by pressure gradients and the Coriolis force. In daytime conditions, the predominant factor is the Coriolis force, which leads to the development of vortex structures. At night, the effect of pressure changes intensifies, which causes disturbances propagate to lower latitudes in the longitude sector depending on the spatial scales of the disturbance region. The circulation disturbance is complex. In this case, the wind mechanism does not play a decisive role in forming a negative disturbance because the prevailing wind speed directions, primarily the meridional one, are not formed.

It is known that the development of ionospheric disturbances at the F-region heights is influenced by the processes of meridional transport and changes in neutral composition, mainly the atomic oxygen to molecular nitrogen concentration ratio $n[O]/n[N_2]$. Thermal heating in the thermosphere causes $n[O]/n[N_2]$ to decrease and negative TEC perturbations to occur. Consider how the $n[O]/n[N_2]$ ratio changed in our calculations.

Figure 8 illustrates distributions of $\Delta(n[O]/n[N_2])$ at an altitude of 200 km for 12:00 UT on October 29 and 30, 2017. It is clearly seen that due to neutral gas heating $n[O]/n[N_2]$ decreases significantly, and the range of negative values of $\Delta(n[O]/n[N_2])$ expands and shifts to low latitudes. Note that the region of decrease in $n[O]/n[N_2]$ does not completely coincide with the region of negative perturbations of ΔTEC, although their location is very close.

To compare the model results of the $n[O]/n[N_2]$ change with the experiment, we have used data obtained with the Global UltraViolet Imager (GUVI) on the TIMED (Thermosphere–Ionosphere–Mesosphere Energetics and Dynamics) satellite [Strickland et al., 1995]. The GUVI data allows us to calculate the ratio between integral concentrations of atomic oxygen and molecular nitrogen in a certain altitude range (generally from 130 to 165 km). We employed level 3 data available on the website [https://guvitimed.jhuapl.edu]. For comparison with model calculations, a data set for the longitude sector 0°–30° E and the time interval from 08:00 to 12:00 UTC was selected and averaged over 15 days (from October 23 to November 6, 2017). Figure 9 shows two latitude profiles of $n[O]/n[N_2]$ according to TIMED/GUVI data — for the meteorologically disturbed day on October 30 and averaged over October 23 – November 6.

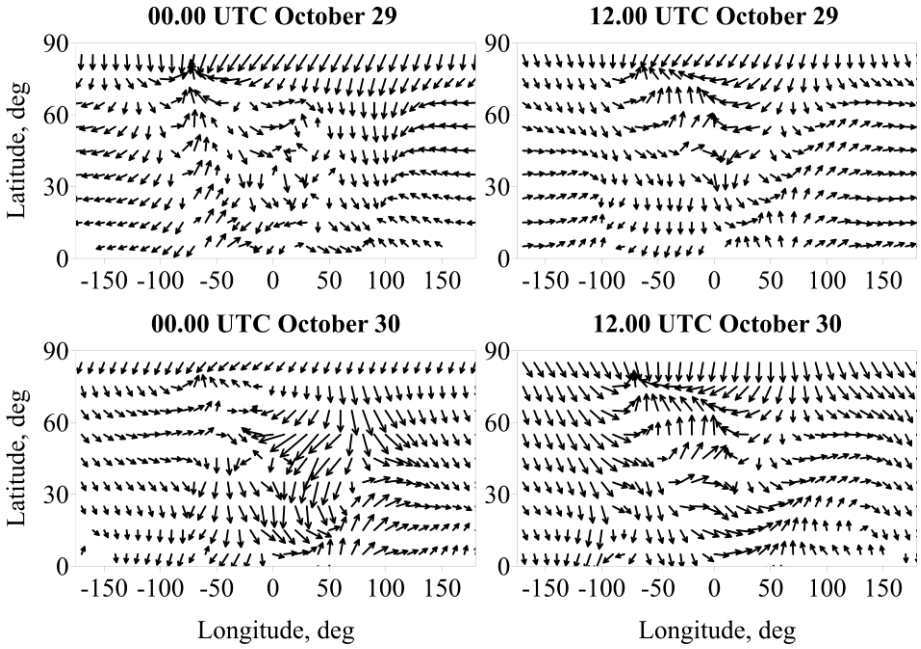

Figure 7. Perturbation of the horizontal velocity vector of neutral gas ΔV at an altitude of 250 km on October 29–30, 2017

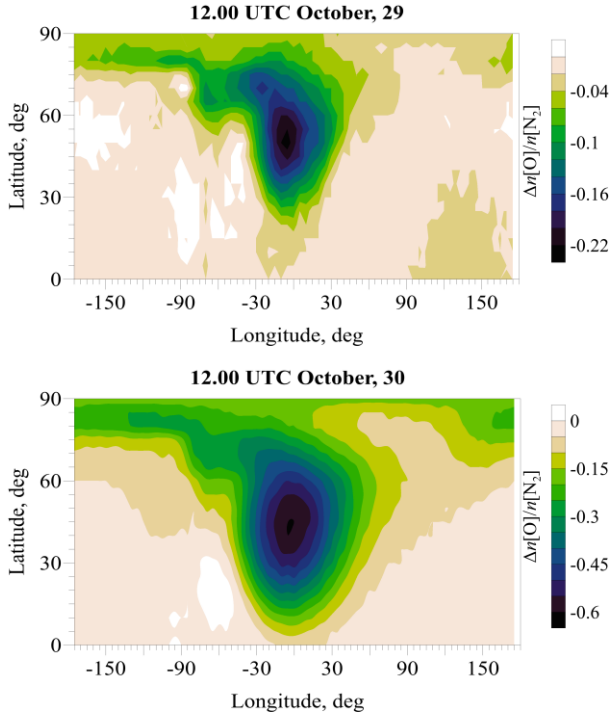

Figure 8. Change in the $n[O]/n[N_2]$ ratio at an altitude of 200 km at 12:00 UT on October 29 (*a*) and 30 (*b*), 2017

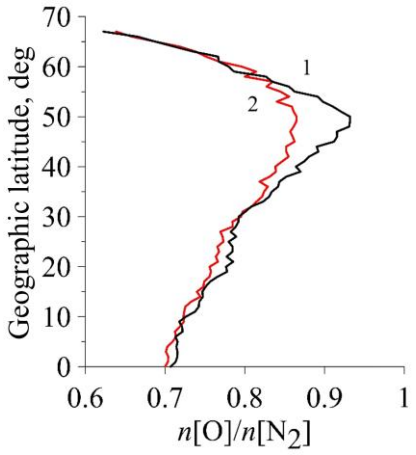

Figure 9. Latitudinal profiles of the integral ratio $n[O]/n[N_2]$ according to GUVI/TIMED satellite data in the longitude range 0°–30° E: 1 — averaged over October 23 – November 6; 2 — on the meteorologically disturbed day on October 30

It can be seen that at latitudes 35°–55° N, which correspond to the region of the meteorological disturbance, on October 30 $n[O]/n[N_2]$ decreases by ~10 % according to TIMED/GUVI data as compared to average data. Note that geomagnetic conditions during the period of interest were undisturbed.

CONCLUSION

The results of numerical experiments on modeling ionospheric effects of the October 28–30, 2017 meteorological storm have shown that a local additional thermospheric heating source generates perturbations of medium parameters both directly above the source and at a considerable distance from it. The physical processes that determine the ionospheric response in the immediate vicinity of the source are caused by the heating of the thermosphere and its effect on dynamic processes, as well as on changes in the neutral composition of the ionosphere. A zone of negative ionospheric effects is formed in the heating region. In regions remote from the source, changes are caused by transport processes associated with pressure changes and the action of the Coriolis force. This leads to motion of plasma to the east and shift of ionospheric anomalies to low latitudes. The influence of these factors is determined by significant spatial scales of the additional heat source and the duration of its operation. Notice that the resulting disturbances in the thermospheric wind circulation are not the main factor responsible for the ionospheric response to these changes.

In general, our findings show the following:

1. Directly in the region of additional heating of the thermosphere, a decrease in Δ*TEC* during the daytime on October 29 and 30 runs to 20 % compared to the quiet day. At night, *TEC* perturbations are negligible.

2. South and east of the additional source, positive Δ*TEC* perturbations with relative amplitudes 5–10 % occur during the daytime. On prolonged exposure to the heat source, the regions of positive perturbations shift to equatorial latitudes.

3. Perturbations of the thermospheric wind circulation are not the main factor determining the ionospheric response to the disturbances considered. Hence it follows that a change in the gas composition of the thermosphere plays an important role. Compared to the experimental data, our calculations demonstrate a 2–2.5-fold decrease in $n[O]/n[N_2]$ as opposed to observational data, which causes a much stronger ionospheric disturbance than in observations. The reason for this may be insufficient knowledge about characteristics of the source of thermospheric disturbances during meteorological storms.

The research was financially supported by the Russian Science Foundation (Grant No. 25-27-00213) [https://rscf.ru/project/25-27-00213/].

REFERENCES

Artru J., Ducic V., Kanamori H., et al. Ionospheric detection of gravity waves induced by tsunamis. *Geophysical Journal International*. 2005, vol. 160, iss. 3, pp. 840–848. DOI: 10.1111/j.1365-246X.2005.02552.x.

Astafyeva E. Ionospheric detection of natural hazards. *Rev. Geophys*. 2019, vol. 57, pp. 1265–1288. DOI: 10.1029/2019RG000668.

Bessarab F.S., Koren'kov Yu.N. Effect of nitric oxide on global distributions of thermospheric and ionospheric parameters. *Geomagnetizm i aeronomiya* [Geomagnetism and Aeronomy]. 1998, vol. 38, no. 5, pp. 645–651. (In Russian).

Bishop R.L., Aponte N., Earle G.D., et al. Arecibo observations of ionospheric perturbations associated with the passage of tropical storm Odette. *J. Geophys. Res.* 2006, vol. 111, iss. A11, no. 320, pp. 1–9. DOI: 10.1029/2006JA011668.

Chernigovskaya M.A., Shpynev B.G., Ratovsky K.G. Meteorological effects of ionospheric disturbances from vertical radio sounding data. *J. Atmos. Solar-Terr. Phys*. 2015, vol. 136, pp. 235–243. DOI: 10.1016/j.jastp.2015.07.006.

Gavrilov N.M., Koval A.V., Kshevetskii S.P. Thermal effects of nonlinear acoustic-gravity waves propagating at thermospheric temperatures matching high and low solar activity. *J. Atmos. Solar-Terr. Phys*. 2020, vol. 208, p. 105381. DOI: 10.1016/j.jastp.2020.105381.

Hersbach H., Bell B., Berrisfordand P., et al. The ERA5 global reanalysis. *Quarterly Journal of the Royal Meteorological Society*. 2020, vol. 146, iss. 730, pp. 1999–2049. DOI: 10.1002/qj.3803.

Hickey M.P., Schubert G., Walterscheid R.L. Acoustic wave heating of the thermosphere. *J. Geophys. Res*. 2001, vol. 106, iss. A10, pp. 21543–21548. DOI: 10.1029/2001JA000036.

Hickey M.P., Walterscheid R.L., Schubert G. Gravity wave heating and cooling of the thermosphere: Roles of the sensible heat flux and viscous flux of kinetic energy. *J. Geophys. Res*. 2011, vol. 116, p. A12326. DOI: 10.1029/2011JA016792.

Karpov I.V., Vasiliev P.A. Ionospheric disturbances due to the influence of localized thermospheric sources. *Geomagnetism and Aeronomy*. 2020, vol. 60, no. 4, pp. 477–482. DOI: 10.1134/S0016793220040064.

Karpov I.V., Radievsky A.V., Kshevetsky S.P., et al. Disturbances of the upper atmosphere and ionosphere caused by acoustic-gravity wave sources in the lower atmosphere. *Russ. J. Phys. Chem. B*. 2016, vol. 10, no. 1, pp. 127–132. DOI: 10.1134/S199079311601005X.

Karpov I.V., Borchevkina O.P., Vasilev P.A. Simulation of ionospheric effects induced by meteorological storms. *Russ. J. Phys. Chem. B*. 2020, vol. 14, no. 2, pp. 362–366. DOI: 10.1134/S1990793120020220.

Klimenko M.V., Bryukhanov V.V., Klimenko V.V. Numerical simulation of the electric field and zonal current in the Earth's ionosphere: The dynamo field and equatorial electrojet. *Geomagnetism and Aeronomy*. 2006, vol. 46, no. 4, pp. 457–466. DOI: 10.1134/S0016793206040074.

Klimenko M.V., Klimenko V.V., Zakharenkova I.E., et al. Formation mechanism of great positive TEC disturbances prior to Wenchuan earthquake on May 12, 2008. *Adv. Space Res*. 2011, vol. 48, no. 3, pp. 488–499. DOI: 10.1016/j.asr.2011.03.040.

Klimenko M.V., Klimenko V.V., Zakharenkova I.E. Longitudinal variations of the ionospheric, plasmaspheric, and total electron contents in December 2009. *Russ. J. Phys. Chem. B*. 2016, vol. 10, pp. 100–108. DOI: 10.1134/S1990793116010085.

Korenkov Yu.N., Bessarab F.S., et al. Numerical modelling of the thermosphere-ionosphere coupling during substorm. *Adv. Space Res*. 1996, vol. 18, no. 3, pp. 41–44. DOI: 10.1016/0273-1177(95)00834-2.

Koucká Knížová P., Podolská K., Potužníková K., et al. Evidence of vertical coupling: Meteorological storm Fabienne on 23 September 2018 and its related effects observed up to the ionosphere. *Ann. Geophys*. 2020, vol. 38, pp. 73–93. DOI: 10.5194/angeo-38-73-2020.

Koucká Knížová P., Potužníková K., Podolská K., et al. Multi-instrumental observation of mesoscale tropospheric systems in July 2021 with a potential impact on ionospheric variability in midlatitudes. *Frontiers in Astronomy and Space Sciences*. 2023, vol. 10, no. 1197157, pp. 1–22. DOI: 10.3389/fspas.2023.1197157.

Koval A.V., Gavrilov N.M., Kandieva K.K., et al. Numerical simulation of stratospheric QBO impact on the planetary waves up to the thermosphere. *Scientific Reports*. 2022, vol. 12, 21701. DOI: 10.1038/s41598-022-26311-x.

Kurdyaeva Yu., Bessarab F., Borchevkina O., Klimenko M. Model study of the influence of atmospheric waves on variations of upper atmosphere and ionosphere parameters during a meteorological storm on May 29, 2017. *Adv. Space Res*. 2024, vol. 74, no. 5, pp. 2463–2474. DOI: 10.1016/j.asr.2024.05.062.

Lay E. H. Ionospheric irregularities and acoustic-gravity wave activity above low-latitude thunderstorms. *Geophys. Res. Lett*. 2018, vol. 45, pp. 90–97. DOI: 10.1002/2017GL076058.

Li W., Yue J., Yang Y., et al. Analysis of ionospheric disturbances associated with powerful cyclones in East Asia and North America. *J. Atmos. Solar.-Terr. Phys*. 2017, vol. 161, pp. 43–54. DOI: 10.1016/j.jastp.2017.06.012.

Namgaladze A.A, Korenkov Yu.N., Klimenko V.V., et al. Numerical modelling of the thermosphere-ionosphere-protonosphere system. *J. Atmos. Terr. Phys*. 1991, vol. 53, iss. 11-12, pp. 1113–1124. DOI: 10.1016/0021-9169(91)90060-K.

Pancheva D., Mukhtarov P., Smith A. Climatology of the migrating terdiurnal tide (TW3) in SABER/TIMED temperatures. *J. Geophys. Res.-Space*. 2013, vol. 118, pp. 1755–1767. DOI: 10.1002/jgra.50207.

Pedatella N.M., Forbes J.M. Modulation of the equatorial F-region by the quasi-16-day planetary wave. *Geophys. Res. Lett*. 2009, vol. 36, L09105. DOI: 10.1029/2009GL037809.

Pedatella N.M., Liu H.-L. The influence of internal atmospheric variability on the ionosphere response to a geomagnetic storm. *Geophys. Res. Lett*. 2018, vol. 45, pp. 4578–4585. DOI: 10.1029/2018GL077867.

Rahmani Y., Alizadeh M.M., Schuh H., et al. Probing vertical coupling effects of thunderstorms on lower ionosphere using GNSS data. *Adv. Space Res*. 2020, vol. 66, no. 8, pp. 1967–1976. DOI: 10.1016/j.asr.2020.07.018.

Schaer S. *Mapping and predicting the Earth's ionosphere using the global positioning system*: PhD thesis. Bern, University of Bern, 1999, 205 p.

Strickland D.J., Evans J.S., Paxton L.J. Satellite remote sensing of thermospheric O/N2 and solar EUV. 1. Theory. *J. Geophys. Res*. 1995, vol. 100, no. A7, pp. 12217–12226. DOI: 10.1029/95JA00574.

Šindelárova T., Burešová D., Chum J., Hruska F. Doppler observations of infrasonic waves of meteorological origin at ionospheric heights. *Adv. Space Res*. 2009, vol. 43, pp. 1644–1651. DOI: 10.1016/j.asr.2008.08.022.

Yasyukevich A.S., Klimenko M.V., Kulikov Yu.Yu., et al. Changes in the middle and upper atmosphere parameters during the January 2013 sudden stratospheric warming. *Sol-Terr. Phys*. 2018, vol. 4, no. 4, pp. 48–58. DOI: 10.12737/stp-44201807.

Wang J.C., Tsai-Lin R., Chang L.C., et al. Modeling study of the ionospheric responses to the quasi-biennial oscillations of the Sun and stratosphere. *J. Atmos. Solar-Terr. Phys*. 2018, vol. 171, pp. 119–130. DOI: 10.1016/j.jastp.2017.07.024.

Yiğit E., Medvedev A.S. Internal wave coupling processes in Earth's atmosphere. *Adv. Space Res*. 2015, vol. 55, iss. 4, pp. 983–1003. DOI: 10.1016/j.asr.2014.11.020.

Zakharov V.I., Kunitsyn V.E. Regional features of atmospheric manifestations of tropical cyclones according to ground-based GPS network data. Geomagnetism and Aeronomy. 2012, vol. 52, pp. 533–545. DOI: 10.1134/S0016793212040160.

URL: https://guvitimed.jhuapl.edu (accessed date April 16, 2025).
URL: https://rscf.ru/project/25-27-00213/ (accessed date April 16, 2025).

Original Russian version: Karpov I.V., Bessarab F.S., Borchevkina O.P., published in Solnechno-zemnaya fizika. 2025, vol. 11, no. 4, pp. 71–78. DOI: 10.12737/szf-114202507. © 2025 INFRA-M Academic Publishing House (Nauchno-Izdatelskii Tsentr INFRA-M).

How to cite this article

Karpov I.V., Bessarab F.S., Borchevkina O.P. Numerical modeling of spatial perturbations of the ionosphere from local tropospheric sources. *Sol.-Terr. Phys*. 2025, vol. 11, iss. 4, pp. 64–71.
DOI: 10.12737/stp-114202507.